Heliyon 9 (2023) e22552

Contents lists available at ScienceDirect

Heliyon

journal homepage: www.cell.com/heliyon

Metastable FeMg particles for controlling degradation rate, mechanical properties, and biocompatibility of Poly(l-lactic) acid (PLLA) for orthopedic applications

Rafael Guillermo Estrada [a], Marta Multigner [b,*], Natalia Fagali [a,c,d], Rosa María Lozano [d], Marta Muñoz [b], Sandra Carolina Cifuentes [b], Belén Torres [b], Marcela Lieblich [a]

[a] Centro Nacional de Investigaciones Metalúrgicas (CENIM-CSIC), 28040, Madrid, Spain
[b] Universidad Rey Juan Carlos (URJC), 28933, Madrid, Spain
[c] Instituto de Investigaciones Fisicoquímicas Teóricas y Aplicadas (INIFTA), CCT La Plata, CONICET-Facultad de Ciencias Exactas, UNLP, La Plata, Argentina
[d] Cell-Biomaterial Recognition Lab, Department of Cellular and Molecular Biology, Centro de Investigaciones Biológicas Margarita Salas (CIB-MS. CSIC), Madrid, Spain

ARTICLE INFO

Keywords:
PLLA
FeMg
Degradable composite biomaterial
Mechanical properties¸ cytocompatibility
Temporary orthopedic devices

ABSTRACT

Poly(l-lactic) acid (PLLA) is commonly used in bioabsorbable medical implants, but it suffers from slow degradation rate and rapid decline in mechanical properties for orthopedic applications. To address this drawback, recent research has explored the use of Mg as a filler for PLLA, resulting in composites with improved degradation rate and cytocompatibility compared to neat PLLA. In this study, FeMg powder particles were proposed as fillers for PLLA to investigate the potential of PLLA/FeMg composites for bioabsorbable implants. Cylinder specimens of PLLA, PLLA/Fe, PLLA/Mg and PLLA/FeMg were prepared using solvent casting followed by thermo-molding. The microstructure, thermal behavior, *in vitro* degradation behavior in simulated body fluid, mechanical properties and cytocompatibility of these composites were examined. The results indicate that the presence of FeMg particles prevents the deterioration of the composite mechanical properties, at least up to 14 days. Once a certain amount of degradation of the composite is reached, the degradation is faster than that of PLLA. Direct cytotoxicity assays revealed that pre-osteoblast MC3T3-E1 cells successfully adhered to and proliferated on the PLLA/FeMg surface. The inclusion of a low percentage of Mg into the Fe lattice not only accelerated the degradation rate of Fe but also improved its cytocompatibility. The enhanced degradation rate, mechanical properties, and osteoconductive properties of this composite make it a promising option for temporary orthopedic biomedical devices.

1. Introduction

Over the past few decades, there has been a significant quest for temporary orthopedic implants made of appropriate bioabsorbable

* Corresponding author.
E-mail addresses: rafaelem@cenim.csic.es (R.G. Estrada), marta.multigner@urjc.es (M. Multigner), nfagali@inifta.unlp.edu.ar (N. Fagali), rlozano@cib.csic.es (R.M. Lozano), marta.munoz@urjc.es (M. Muñoz), sandra.cifuentes@urjc.es (S.C. Cifuentes), belen.torres@urjc.es (B. Torres).

https://doi.org/10.1016/j.heliyon.2023.e22552
Received 14 June 2023; Received in revised form 7 November 2023; Accepted 15 November 2023
Available online 20 November 2023

and biocompatible materials. Ideally, during bone healing these implants would continuously be substituted by new bone without loss of mechanical strength. Currently, the predominant bioabsorbable osteosynthesis implants available are polymer-based, specifically poly α-hydroxy acids such as poly(l-lactic) acid (PLLA), polyglycolic acid and their copolymers [1]. These materials offer favorable characteristics in terms of biosafety, biodegradability, and malleability. However, they are limited in strength and give rise to acidic byproducts during degradation, potentially leading to aseptic inflammatory responses. PLLA mechanical properties rapidly decline after exposure to a wet environment. However, this drop in mechanical properties is not linked to the degradation of the polymer, which occurs by hydrolysis, but is linked to the diffusion of water within the polymeric chains [2]. In fact, degradation rate of PLLA is very slow. A 5-year in vivo research on the biodegradation of PLLA plates reported the presence of polymeric particles at the implantation site after the 5-year-follow-up. After 5 years of incubation *in vitro* of PLLA plates, samples were not completely degraded and had lost only 52 % of their mass [3]. Up to this point, no single material has proven satisfactory in fulfilling the comprehensive property prerequisites of a bone scaffold [4]. One strategy is to add reinforcing particles to the polymeric matrix [5,6]. Although ceramic particles could be suitable reinforcement candidates, there is some concern about their long-term behavior, as they are mostly biostable or degrade too slowly in physiological environments [7,8]. Metallic particles based on biodegradable biocompatible metals offer a similar approach to ceramic ones. There are three main families of alloys that are being thoroughly investigated for bioabsorbable implants [9]: Mg, Fe and Zn alloys. Mg alloys have emerged as high-strength biodegradable materials, with a few implants already in the market. Fe-based alloys are mainly investigated as vascular stent materials and, more recently, for osteosynthesis applications [10]. The third group is based on Zn, which also presents promising biodegradable properties [11].

In the last few years, composites formed by PLLA and Mg particles have been developed [12–19], which degrade faster than neat PLLA. Additionally, Mg-based fillers prevent the acidification of the medium due to the degradation of the polymer, promote *in vitro* cell proliferation, help regulate the behavior of human mesenchymal stem cells and macrophages, and enhance the osteogenic commitment, as assayed by evaluation of alkaline phosphatase [20–22]. Despite these advantages, PLLA/Mg composites showed limited improvement in mechanical properties. To address this problem, we propose a different reinforcement based on Fe alloys. Fe exhibits a higher Young's modulus and slower degradation rate than Mg. The initial hypothesis is that reinforcing PLLA with Fe-based particles could improve the mechanical properties and modulate the degradation rate in relation to PLLA/Mg composites.

In the present work, the reinforcement particles were selected from the FeMg system. This metastable binary alloy was proposed as biomaterial a few years ago [23], and has since received considerable attention from the research community [24–29]. The hypothesis behind this selection is that a combination of Fe and Mg in solid solution in the Fe-rich range of the phase diagram might present a faster degradation rate than pure Fe [30]. The fact that Fe and Mg are immiscible elements in solid state makes processing of this alloy challenging. To obtain FeMg particles, several out-of-equilibrium techniques have been employed, such as alternate deposition [31], co-evaporation [32], and high energy ball milling [33].

In a previous investigation [29], we prepared metastable FeMg alloys by planetary ball milling and found that the one with 5 wt% of Mg (referred to as FeMg from now on) exhibited the best as-processed characteristics. Upon immersion in Hanks' solution, it was observed that FeMg exhibited higher degradation rate than Fe particles, both milled for 16 h, confirming that Mg had a genuine acceleration effect on the degradation of the alloy.

In the present paper, we used planetary ball milled FeMg particles, as well as Fe and Mg particles, as fillers for a PLLA matrix with the aim of evaluating the composite's suitability as biomaterial for temporary implants. The composites were obtained through a solvent casting route, processed by thermo-molding, and their microstructure, thermal and mechanical behavior, *in vitro* degradation and cytocompatibility were studied.

2. Materials and method

2.1. Processing

The composite materials consisted of a polymeric matrix of PLLA reinforced with particles of either FeMg, Fe, or Mg. The metallic reinforcing particles of FeMg were obtained by a powder metallurgy route in which commercial Fe powder (99.9 % purity, $d < 100$ μm, Goodfellow) and commercial Mg powder (99.8 % purity, $d < 100$ μm, Nitroparis) were milled in a high energy planetary mill (PM-4 Retsch) at 200 rpm for up to 16 h with a powder-to-ball ratio of 7:1 and grinding media of stainless steel balls, 20 mm in diameter. The Fe reinforcing particles were obtained by milling the as-received Fe powder for 16 h (Fe) following the same procedure as with FeMg. Finally, as-received spherical Mg powder particles were used as reinforcement without any modification. Further details about powder processing and their microstructure can be found in Ref. [29].

To prepare the composites, PLLA pellets (Goodfellow) were dissolved in chloroform (analytical grade from Sigma Aldrich, St. Louis, USA) using magnetic stirring at 27 °C. The PLLA solution was then mixed with each powder in a proportion of 6.5 vol% of reinforcement, equivalent to 28 wt% of FeMg, 31.5 wt% of Fe, and 5 wt% of Mg powder. This proportion was chosen to facilitate comparison with results from previous studies [34]. The powders were dispersed into the solutions by sonication for 4 min until a homogeneous appearance was achieved. The resulting solutions were cast in 10 cm diameter molds and left to dry in the air for 48 h to obtain a solid film with 2 mm thickness. To remove the remaining chloroform, the films were heated for 24 h in an oven at 70 °C. Once the films were completely dried, they were cut and ground into small chips using liquid nitrogen.

After obtaining the composite chips, they were introduced into cylindrical molds (6 mm diameter and 9 mm height) and pressed at 190 °C using an Opal 460 hot mounting press (Neurtek) to form cylinders for further characterization. These composite samples are referred to as PLLA/Fe, PLLA/Mg and PLLA/FeMg from now on. Neat PLLA cylinders were also produced by the same methodology for comparison purposes.

2.2. Thermal characterization

Differential scanning calorimetry (DSC) studies were conducted using a TA DSC 25 calorimeter. Samples, weighing about 5 mg, were heated from 0 °C to 200 °C at a rate of 10 °C/min. Prior to the mold pressing process, calorimetric curves of composite chips were obtained to determine their glass transition (Tg) and melting temperature (Tm). Subsequently, calorimetric curves of the hot-pressed cylinders were also obtained, and the crystalline fraction was calculated by the following formula (Eq. 1):

$$f_c = (\Delta Hm - \Delta Hcc)/\Delta Hm^{\circ} \quad (1)$$

where ΔHm refers to the enthalpy of melting, ΔHcc refers to cold crystallization enthalpy, and ΔHm° is the enthalpy of a theoretically 100 % crystalline PLLA. The value used for ΔHm° is 93.1 J/g, as obtained from Lim et al. [35]. For the normalized enthalpy, the following equation (Eq. 2) was used:

$$Hn = (H \bullet Ms) / (M_{PLLA}) \quad (2)$$

where *Hn* is the enthalpy normalized by the actual PLLA mass of the sample, considering the weight percentage of the reinforcement. *H* represents the value of the enthalpy obtained from the DSC, Ms is the total mass of the sample, and M_{PLLA} is the actual mass of PLLA.

2.3. Microstructural characterization

Microstructural characterization of the cylinders was carried out using Scanning Electron Microscopy (SEM) with a HITACHI S4800 microscope equipped with Energy Dispersive X-ray Spectroscopy (EDS). To analyze the cross-section of the specimens, they were longitudinally cut with a diamond disk and cold-mounted using epoxy resin. Final polishing was done with 1 μm diamond paste. For the SEM examination, the specimens were covered with a thin graphite layer.

2.4. In vitro degradation tests

In vitro degradation tests were conducted by immersing the cylinders in modified Dulbecco's phosphate-buffered saline solution (PBS 28374; Thermo Fisher Scientific, Massachusetts, USA) for 14 and 28 days at 37 °C. Degradation behavior was characterized by measuring the mass variation and water absorption. Mass variation was determined by calculating the relative weight difference between the initial sample and the degraded one after drying for 24 h at 50 °C under vacuum. Water absorption was obtained by calculating the relative difference between the mass of the wet specimen measured immediately after withdrawing it from the solution and the dried specimen. Samples were weighed using a precision balance (error of 0.0001 g). Three experiments were conducted for each condition, and the data are presented as mean value ± standard deviation.

2.5. Mechanical characterization

The mechanical behavior of the as-processed and degraded cylinders was studied through compressive tests using a universal machine EM2/100/FR-10kN Micro Tests at ambient conditions. Compression test were after immersing the samples for 14 and 28 days in PBS to assess the effect of *in vitro* degradation on the mechanical performance of the composite. The exact dimensions of each specimen were measured before each compression test. Experiments were conducted in triplicate using a strain rate of 5×10^{-3} s^{-1} (crosshead speed 2.60 ± 0.07 mm/min, sample height 8.5 ± 0.3 mm), and a displacement sensor (Schreiber Messtechnik, model SM224.2.2R) was used to measure the deformation. Young's modulus and compression yield strength were obtained from the stress/strain curves. Data are presented as mean value ± standard deviation.

2.6. Cytotoxicity assays

The mouse pre-osteoblast MC3T3-E1 cell line was obtained from the DSMZ Human and Animal Cell Bank (Braunschweig, Germany). Cells were cultured in DMEM medium (DMEM 41966; Gibco, Life Technologies Limited, Paisley, UK) with 10 % heat-inactivated fetal bovine serum (FBS; Sigma, St. Louis MO, USA) and a mixture of antibiotics (penicillin 100 units/mL and streptomycin 100 μg/mL; Gibco, Life Technologies Limited, Paisley, UK). The cells were maintained r at 37 °C and 5 % CO_2 in a cell culture chamber.

PLLA, PLLA/Fe, PLLA/Mg, and PLLA/FeMg cylinders (0.5 cm diameter, 0.196 cm^2 area) were sterilized under UV-light irradiation for 15 min on a 24-well culture plate in a laminar flow cabinet to maintain sterility. For direct cytotoxicity assays, 4080 pre-osteoblast cells MC3T3-E1 were seeded on each sample (20800 cells/cm^2 cell density) and incubated for 24 h.

Cytocompatibility was evaluated through calcein-AM/Hoechst double staining technique as described in a previous work [36]. Calcein-AM dye (C3100MP, Thermo Fisher; Ex/Em 494/515 nm) stains intact cells green. It can pass through the cell membrane and fluoresce when the ester groups in the dye molecule are removed by intracellular esterases. On the other hand, Hoechst (2,7-Hoechst 33258, Sigma Aldrich; Ex/Em 350/461 nm) labels DNA from the nuclei of dead cells, which can be detected by fluorescence microscopy.

For this assay, samples were incubated with 1 mL of a mixture of dyes (0.5 μM of each) in DMEM culture medium without FBS for 20 min, in darkness. Then, the cells were washed with PBS twice and observed with a fluorescence microscope (Leica).

3. Results

3.1. Thermal characterization of solvent cast materials

Fig. 1a,b shows the DSC curves of PLLA and the three composite materials (PLLA/FeMg, PLLA/Fe and PLLA/Mg) under study. Table 1 and Table 2 list the thermal properties derived from the solvent cast samples and the hot-pressed cylinders, respectively.

The DSC curves of solvent cast materials showed the glass transition followed by the endotherm due to the melting process. PLLA and composites showed the Tg around 50 °C and the Tm around 150 °C. In all cases, the melting process has been completed at temperatures below 170 °C. The absence of a cold crystallization peak reveals that the solvent casting process resulted in highly crystalline PLLA samples.

Regarding thermo-moulded samples, DSC curves show first the glass transition followed by an exotherm due to cold crystallization and an endotherm given by polymer melting. The small fc value obtained suggests that the cooling rate was fast enough to prevent the crystallization of the polymer, resulting in amorphous materials. A change in the Tg was evident for the Fe-reinforced composite, with an increase of 4 °C compared to the Tg of PLLA. This indicates that the chain mobility of the polymer is affected by Fe particles. Metallic particles containing Mg accelerated the cold crystallization of PLLA. Table 2 shows that Tcc of composites reinforced with Mg and FeMg were between 3 and 4 °C lower than Tcc of pure PLLA. The melting peak was characterized by a bimodal behavior that could be attributed to a melting-recrystallization phenomenon [34]. For PLLA and PLLA/Fe, this bimodal behavior was characterized by a melting peak accompanied by a shoulder at higher temperatures. For PLLA/Mg and PLLA/FeMg, two melting peaks were clearly revealed. The first melting peak (Tm1) of the three composites appeared at a temperature that was 1–2 °C lower than that of PLLA, whereas there was no significant difference between the composites and PLLA in the second melting peaks (Tm2) values.

3.2. In vitro degradation tests

Fig. 2 shows the cylindrical specimens as-processed (a.p.) and after immersion during 14 and 28 days in PBS. The as-processed samples exhibited a smooth and homogeneous surface, with neat PLLA appearing as a translucent body, while metallic reinforcement resulted in opaque dark cylinders. It was also observed that the particles have not undergone any visible oxidation reaction during the thermomechanical processing of the specimens. After 14 days of immersion in PBS, the differences between the materials became evident due to the presence of various degradation products on their surfaces. Unreinforced PLLA showed no significant change, whereas grayish spots appeared in the Mg-reinforced PLLA, yellowish stains in PLLA/Fe, and a mixture of both types of reaction products in PLLA/FeMg. After 28 days of immersion, the effect of degradation was more pronounced, with noticeable increase in the amount of reaction products on the surfaces of the three composites and a clear swelling of the cylinder in the case of the PLLA/FeMg composite.

Fig. 3 displays longitudinal sections of non-degraded composite samples: PLLA/Mg, PLLA/Fe and PLLA/FeMg in (a), (d) and (g), respectively. In Fig. 3 (a), a relatively uniform distribution of particles is observed, while the other two materials showed some particle agglomerates. Fig. 3 (b), (e) and (h) show the composite samples degraded for 14 d, and Fig. 3 (c), (f) and (i) show the samples degraded for 28 days of immersion. As the degradation time increased, the specimen edges became less defined, and the metallic particles exhibited partial or complete oxidation, evident by the decreasing fraction of particles with bright contrast.

Fig. 4 shows the cross-section of PLLA/Mg after (a) 14 days and (b) 28 days of degradation. The degradation of this composite after 14 days was evident only in particles located very close to the surface, which appeared surrounded by a reaction phase (gray color)

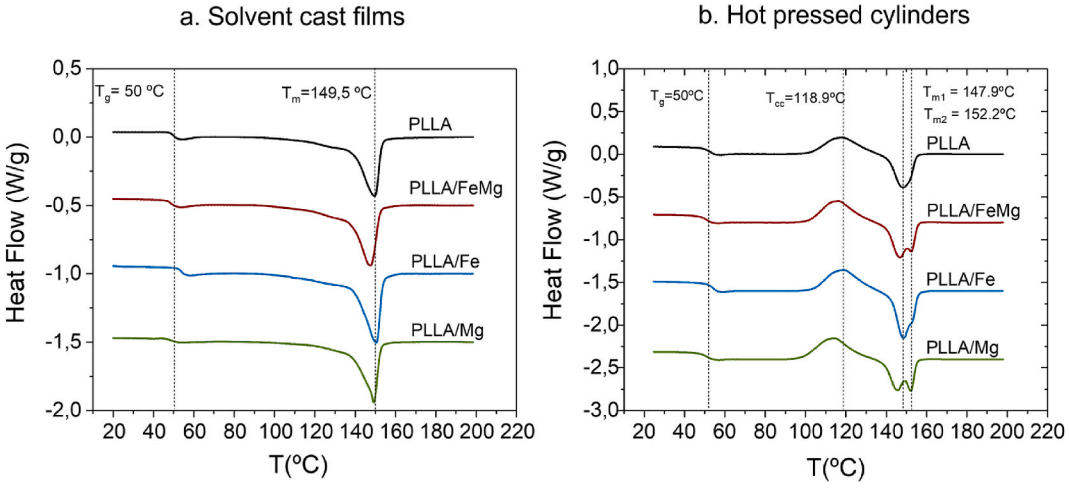

Fig. 1. DSC scans of PLLA composites reinforced with 6.5 vol% of FeMg, Fe and Mg particles: (a) obtained by solvent casting and (b) after hot pressing process to form cylinders. Reference lines have been added as guides for better visualization.

Table 1
Thermal properties of materials obtained by solvent casting: Glass transition temperature (T_g), melting temperature (T_m), enthalpy of melting (ΔH_m), and crystalline fraction (f_c). Experimental errors: $T_g \pm 2$ °C, $T_m \pm 0.5$ °C, and $f_c \pm 0.04$

Sample	T_g (°C)	T_m (°C)	ΔH_m(J/g)	f_c
PLLA	50	149.5	35.0	0.38
PLLA/Mg	49	148.9	32.1	0.34
PLLA/Fe	54	150.2	45.1	0.48
PLLA/FeMg	49	147.3	39.4	0.42

Table 2
Thermal properties of hot-pressed cylinders: Glass transition temperature (T_g), Cold crystallization temperature (T_{cc}), melting temperature of the first peak (T_{m1}), melting temperature of the second peak (T_{m2}), enthalpy of melting (ΔH_m), and crystalline fraction (f_c). Experimental errors: $T_g \pm 2$ °C, T_{cc} and $T_m \pm 0.5$ °C, and $f_c \pm 0.04$

Sample	Tg (°C)	T_{cc} (°C)	T_{m1} (°C)	T_{m2} (°C)	ΔH_m (J/g)	f_c
PLLA	50	118.9	147.9	152.2	1.4	0.02
PLLA/Mg	51	114.5	145.7	152.2	1.7	0.02
PLLA/Fe	54	118.8	146.7	152.3	4.7	0.05
PLLA/FeMg	50	115.5	146.6	152.2	1.2	0.01

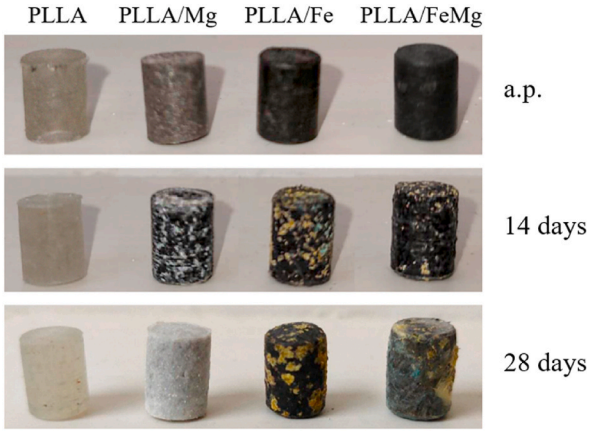

Fig. 2. Photographs of the cylinders (6 mm diameter, 9 mm height) in their as-processed and degraded states after 14 and 28 days of immersion in PBS. From left to right: PLLA, PLLA/Mg, PLLA/Fe and PLLA/FeMg.

identified as $Mg(OH)_2$ [15]. After 28 days (Fig. 4b), particles near the surface appeared to be fully transformed, and even those at about 1 mm from the surface showed signs of reaction with PBS. The fact that the corrosion reaction was faster in particles located at the surface and subsurface of the cylinders than in particles situated in the core of the specimens indicates a gradient in the degradation process, which can be attributed to a gradual diffusion of PBS into the cylinders' volume. Fig. 4 also reveals matrix/particle interface deterioration, as indicated by holes left by particles during the metallographic preparation of the sample for SEM observation. Another feature that was observed after 28 days of degradation is the presence of strings of $Mg(HO)_2$ (Fig. 4b, black arrow) due to its dissolution and re-precipitation. This effect was also reported by Cifuentes et al. [12].

Fig. 5 shows the PLLA/Fe composite after 28 days of immersion in PBS. All particles at the periphery displayed signs of reaction with the solution, and large deposits covered the sample surface. Inside the cylinder, only particles close to the surface underwent transformation, resulting in a compact oxide layer, which protected the specimen from further reactions by preventing the entrance of the PBS solution. EDS analysis of the surface products revealed the presence of Na and P, in addition to Fe, C and O, while no P or Na was found in particles further inside the cylinders.

Fig. 6 shows SEM images of PLLA/FeMg composites after 28 days of immersion in PBS. Similarly, to what occurred in PLLA/Fe samples, reactions mainly occurred on the surface and subsurface particles. Even after 14 days of degradation, sparse oxides aggregates appeared at the surface. They appeared mainly in two forms, as plates (Fig. 6a) and as a bundle of needles (Fig. 6b). Both types of products contained Na and P, in addition to Fe, Mg, C and O, as observed in PLLA/Fe except for Mg. This suggests that they were formed mainly as a reaction with Fe. Contrary to what occurred to PLLA/Fe in PLLA/FeMg composite, these surface oxides did not restrict diffusion of PBS, which penetrated more deeply inside the cylinder, thereby increasing its degradation. In this case, P was not detected in particles inside the cylinder.

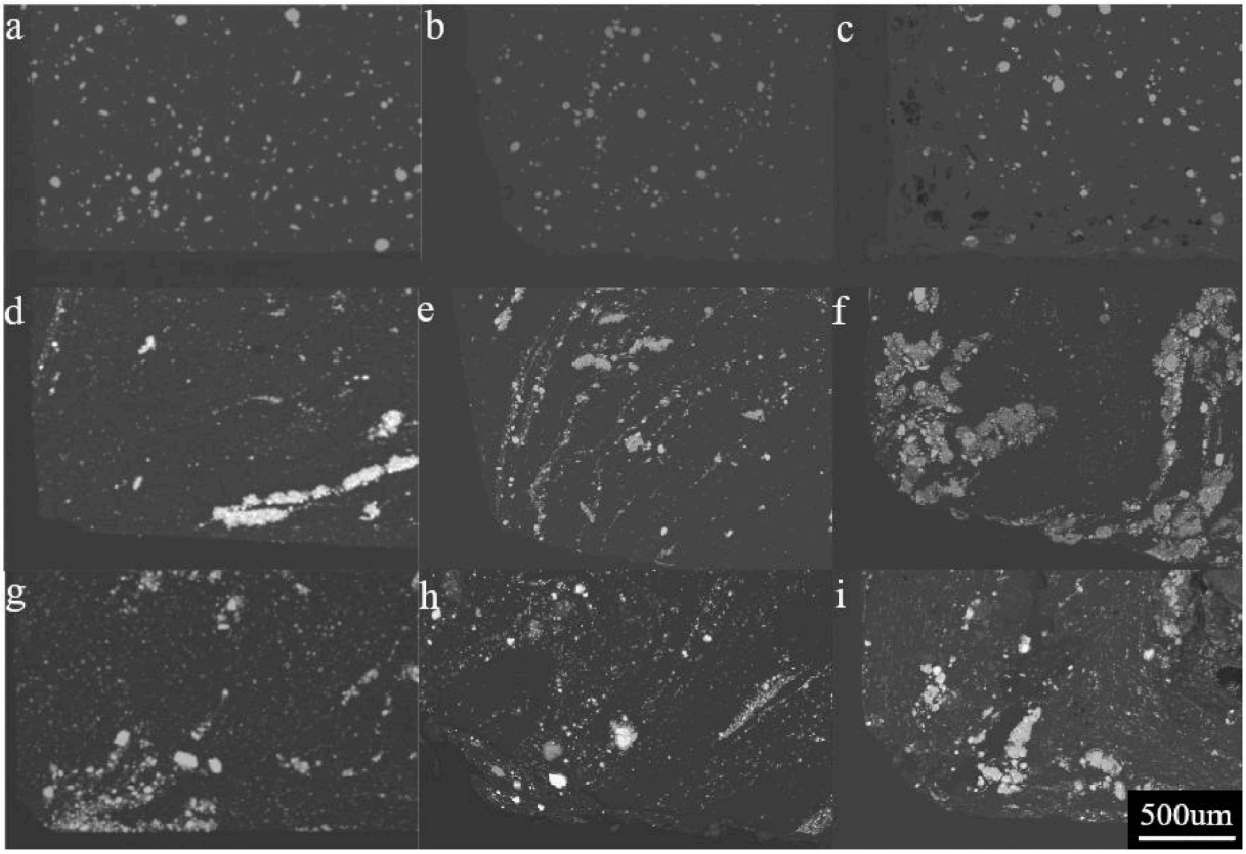

Fig. 3. Low-magnification backscattered electron images of as-processed composites: PLLA/Mg, with (a) as-processed, (b) after 14 days, and (c) after 28 days of immersion; PLLA/Fe, with (d) as-processed, (e) after 14 days, and (f) after 28 days of immersion in PBS; and PLLA/FeMg, with (g) as-processed, (h) after 14 days, and (i) after 28 days of immersion.

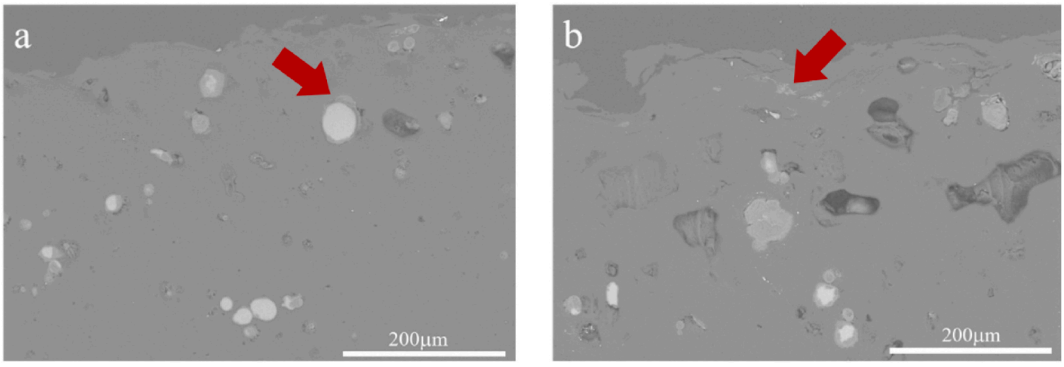

Fig. 4. Backscattered electron images of PLLA/Mg sample after (a) 14 days and (b) 28 days of immersion in PBS. Bright contrast particles indicate the presence of Mg. The gray particles corresponds to the $Mg(OH)_2$ reaction product (examples shown by red arrows).

3.3. Water intake and mass variation

During degradation, liquids diffuse into the samples in varying amounts depending on the degradation mechanism. This water intake is reflected in an increase in weight compared to the dry degraded sample. Fig. 7 (a) shows the water absorption for the polymer sample (PLLA) and the composites (PLLA/Mg, PLLA/Fe and PLLA/FeMg) after 14 and 28 days of immersion in PBS. In general, a higher a weight gain suggests a higher degradation rate. PLLA and PLLA/Fe showed a similar behavior, with a water absorption of 1.77 wt% and 2.46 wt% respectively after 14 d. On the other hand, PLLA/Mg and PLLA/FeMg retained 4.65 wt% and 4.82 wt%, respectively, which is about twice as much, indicating that these materials allow greater penetration of the solution. After 28 days, the trend

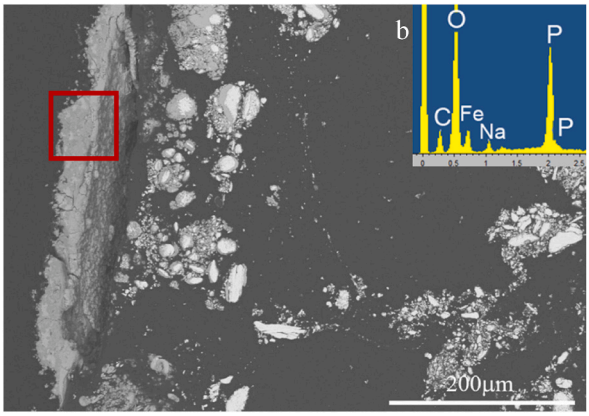

Fig. 5. SEM micrograph of PLLA/Fe after 28 days of degradation. Inset: EDS analysis of the surface reaction product (marked region).

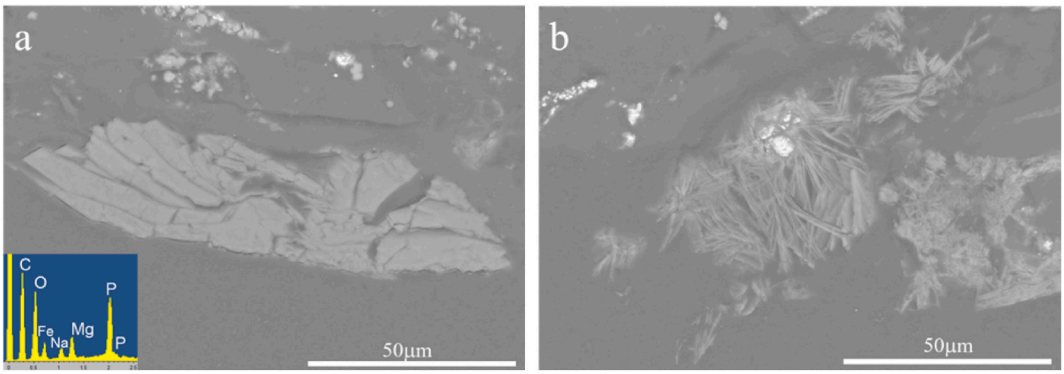

Fig. 6. Micrographs of PLLA/FeMg after 28 days of degradation showing two types of corrosion products: (a) plate, and (b) bundles of needles. Inset: EDS of degradation products.

remained similar but with a larger difference between the two groups of composites. While PLLA and PLLA/Fe retained similar weight percentage (1.84 and 3.51 wt%, respectively), PLLA/Mg adsorbed 11.64 wt% of the solution and PLLA/FeMg adsorbed 14.27 wt%, which is about four to five times more than PLLA and PLLA/Fe, respectively. The high dispersion in the data of the water intake of PLLA/FeMg composites after 28 days of immersion is a consequence of the high degradation level of the polymeric matrix. That has been observed in bulk eroded polymers as poly-(l,d-lactic) acid [37].

Fig. 7 (b) shows the outcomes of mass variation, which refers to the weight difference between the initial dry samples and the dry samples that have undergone degradation. These results offer insights into both the extent of material loss to the surrounding media and the quantities of new phases that have emerged and persisted within the samples. Following a 14 days immersion period, minimal mass variation was observed in PLLA and PLLA/Fe samples. In contrast, PLLA/Mg and PLLA/FeMg experienced weight increases of

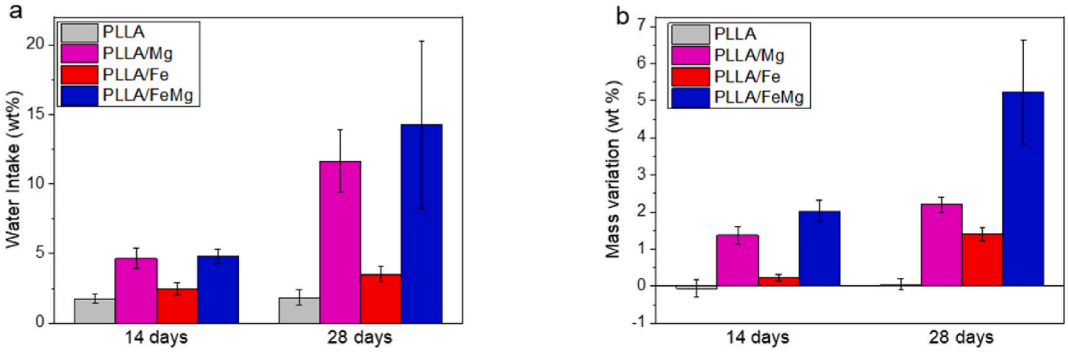

Fig. 7. (a) Water intake and (b) mass variation after 14 days and 28 days of immersion in PBS for PLLA, PLLA/Mg, PLLA/Fe and PLLA/FeMg composites.

1.37 wt% and 2.02 wt%, respectively. Over a span of 28 days, the extent of mass variation diverged among the three composite types: from 1.37 wt% to 2.2 wt% in the case of PLLA/Mg, from 0.23 to 1.4 wt% for PLLA/Fe and from 2.02 to 5.23 wt% for PLLA/FeMg, it is worth highlighting that the latter composite exhibited the most substantial gain in mass.

3.4. Mechanical properties

Uniaxial compression tests were conducted on both neat PLLA and the three composite materials, both in their as-processed state and after undergoing 14 and 28 days of immersion in PBS for degradation. Fig. 8 illustrates the representative stress-strain curves for each material and timeframe. All the curves exhibited the characteristic behavior of amorphous polymers: an initial linear stress increase at low strain (elastic region), a transition to non-linear behavior with a peak stress (yield point), subsequent strain softening leading to a plastic flow regime marked by a plateau, and finally, strain hardening due to chain deformation [38]. The degree of strain softening decreased while the level of strain hardening increased with degradation for all materials. Particularly, materials reinforced with metallic particles experienced a more pronounced increase in strain hardening over time. At 28 days, composite materials displayed reduced softening, enhanced hardening, and heightened mechanical resilience during the post-yield phase compared to neat PLLA. This indicates that the inclusion of metallic particles imparts a strengthening effect on the PLLA matrix as degradation progresses.

Fig. 9 (a) illustrates the compressive modulus (E) values over immersion time. Generally, E declines due to polymer chain degradation. However, accounting for the error bars, in the a.p. state, PLLA, PLLA/Mg and PLLA/FeMg samples exhibited comparable E values (ranging from 2.7 to 3.2 GPa), whereas PLLA/Fe displayed a slightly lower stiffness (2.1 GPa). After 14 days of degradation, all E moduli fell within the range of 1.8–2.8 GPa. Following 28 days of immersion, the compressive modulus of neat PLLA remained at 2 GPa, while those of the three composites decreased to 1.3–1.6 GPa, nearly half of their original values. With regards to the compressive strength (Fig. 9b), PLLA presented the highest strength in the a.p. state (100 MPa), around 20 MPa higher than that of the composites. After 14 days in PBS, the four materials presented yield strengths of around 80 MPa. After 28 d, only the PLLA/FeMg composite experienced a significant reduction in yield strength (46 MPa).

To highlight the evolution of the compressive elastic modulus and the yield strength of each material, it is interesting to refer them to the values of each as-processed cylinders, i.e. to divide them by their initial as-processed value multiplied by 100. These normalize values are represented in Fig. 10 (a,b).

It is evident that following 14 days of degradation, PLLA experienced a significant decline in its mechanical properties and appeared to reach a plateau. In contrast, the metal-reinforced materials retain their initial mechanical properties after the initial 14 days of degradation, and it is only after 28 days that a notable reduction in both strength and modulus becomes apparent. This effect is particularly pronounced in the case of the yield strength of PLLA/FeMg.

3.5. Cytotoxicity assays

Direct cytotoxicity assays employing calcein-AM/Hoechst double staining, have unveiled significant variations in the cytocompatibility profiles of PLLA and its diverse composite materials.

The micrographs of the PLLA control group (Fig. 11) show a substantial population of green-stained viable cells ($\bar{x} = 282$) with a low number of deceased cells, indicated by blue nuclei ($\bar{x} = 4$), accounting for 1 % of the total. The cells interfacing with the PLLA displayed an expansive cytoplasm, extending filopodia and demonstrated robust adhesion to the material surface.

In contrast, the ability of cells to attach and survive on the surfaces of PLLA/Fe and PLLA/Mg composites was notably restricted ($\bar{x} = 130$ and 44, respectively). These composites presented a higher number of dead cells ($\bar{x} = 10$ in both cases) when compared to PLLA.

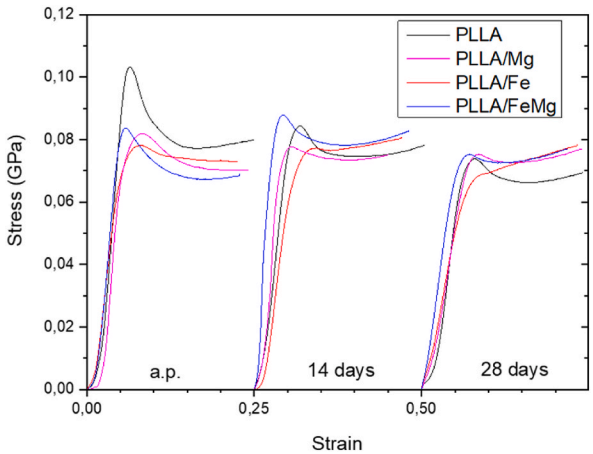

Fig. 8. Representative stress-strain curves for each material and degradation time.

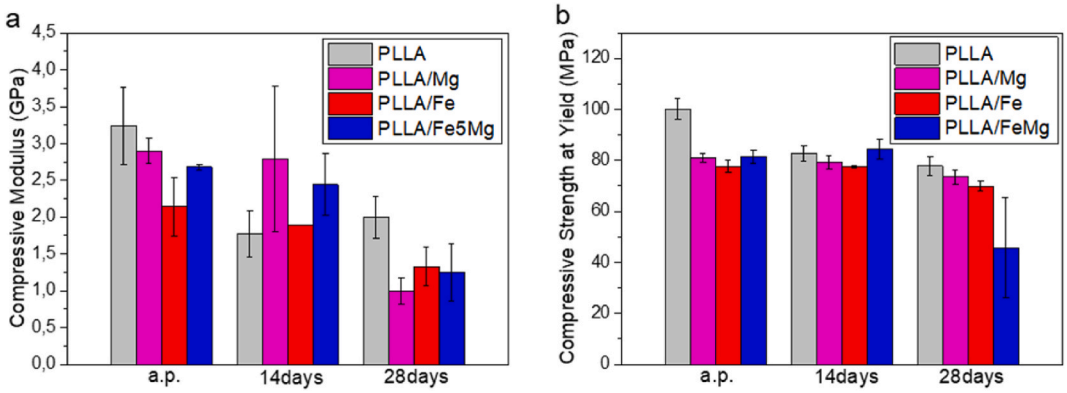

Fig. 9. Variation in (a) compressive modulus, and (b) compressive strength at yield for neat PLLA and its composites over degradation time.

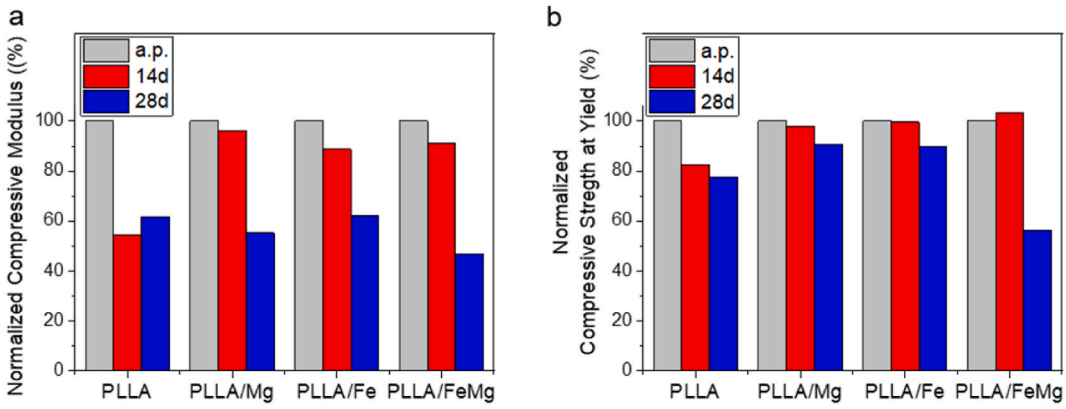

Fig. 10. (a) Compressive modulus, and (b) yield compressive strength of neat PLLA and the three composites as a function of immersion time, normalized (%) by their own as-processed values.

This resulted in death rates of 7 % and 18 % for PLLA/Fe and PLLA/Mg, respectively. The micrographs demonstrate cell morphologies characterized by condensation, shrinkage, and rounded appearance, with a more pronounced effect observed in the case of PLLA-Mg.

Cell morphology on PLLA/FeMg resembled that observed in PLLA/Fe scenario, with a smaller and more compact appearance relative to the PLLA surface. Remarkably, a significant number of pre-osteoblast MC3T3-E1 cells seeded on PLLA/FeMg successfully attached and proliferated on the surface ($\overline{x} = 194$), accompanied by a minor number of deceased cells ($\overline{x} = 14$) that represents 7 % of death.

4. Discussion

In the development of biodegradable implants, it is imperative not only for the material to be well-tolerated by the body, but also for it gradually dissolve as the patient recovers. Currently, degradable polymers, primarily PLLA and polyethylene glycol acid, find application as plates, pins, and similar devices. While these materials meet the essential criterion of biocompatibility, their degradation rate often proves to be too slow, and their mechanical strength insufficient. In this study, we introduced PLLA/FeMg as an innovative biodegradable material. To initiate a preliminary assessment of its viability, we explored three primary attributes: degradation rate, mechanical strength and cell compatibility alongside their counterparts in neat PLLA. Furthermore, we also fabricated two additional composites, PLLA/Mg and PLLA/Fe, to discern and analyze the distinct influence of each metal powder.

Sample degradation was tracked through measurement of mass variation and water absorption (Fig. 7). Notably, PLLA/FeMg exhibited the most substantial values. Within this composite, the metallic particles distributed throughout the cylinder volume reacted with the pseudo-physiological medium, resulting in reaction products that contributed to an increase in sample weight. Conversely, the heightened water absorption signifies the deterioration of polymer chains. Both of these characteristics collectively point to a swifter degradation rate for PLLA/FeMg when compared to the other materials. While the most pronounced changes were observed in PLLA/FeMg samples, the other two composites also displayed weight increases. This phenomenon is particularly evident in the case of PLLA/Mg, where the water uptake after 28 days surpassed that of the 14 days interval, indicating significant matrix degradation, exceeding that observed in the PLLA/Fe scenario. Reaction products present on the surface of the PLLA/Fe sample acted as protective layers, impeding the ingress of liquid medium and thus retarding the degradation of PLLA.

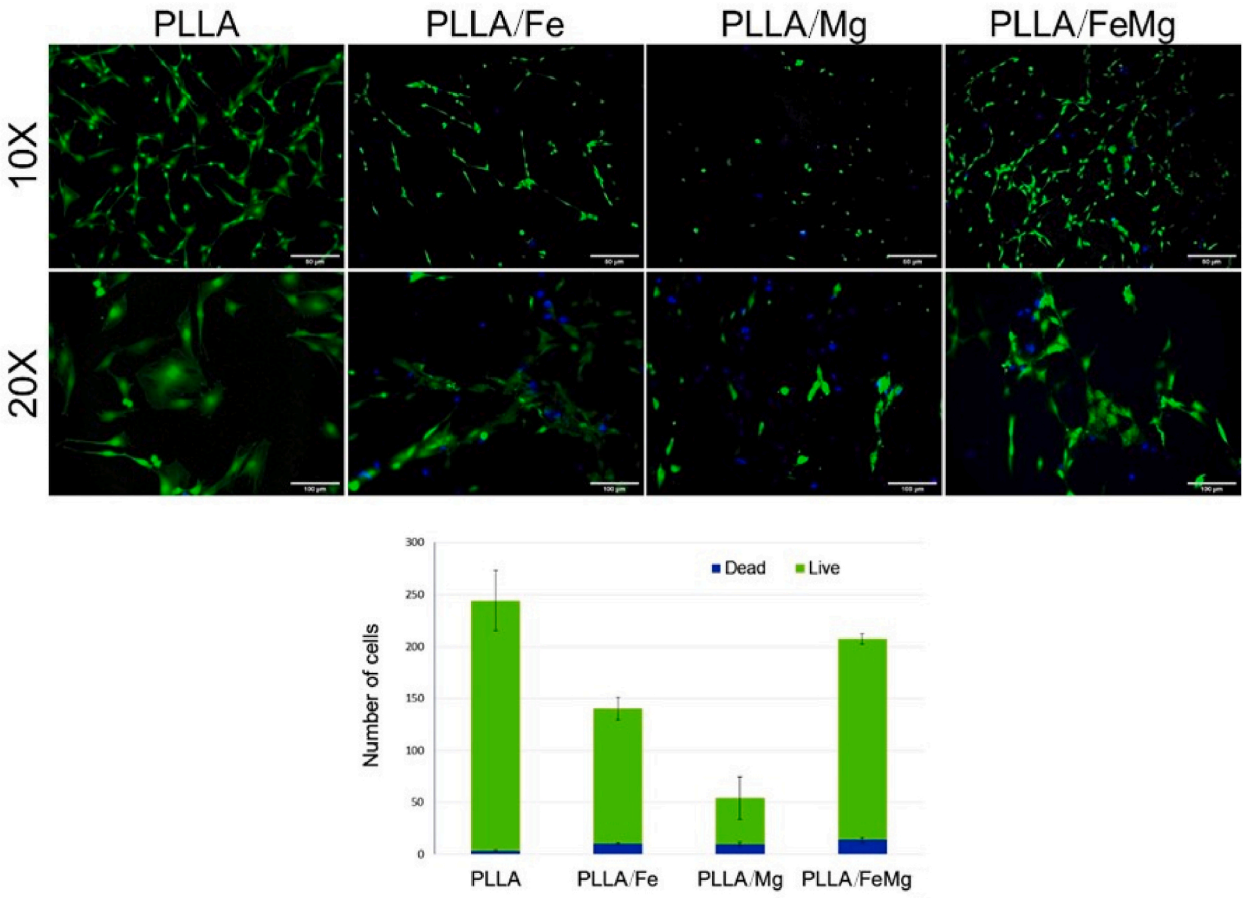

Fig. 11. Assessment of cytocompatibility for MC3T3-E1 cells on PLLA, PLLA/Fe, PLLA/Mg and PLLA/FeMg. Live cells are highlighted in green using Calcein-AM staining, while damaged or deceased cell nuclei are marked in blue with Hoechst 33258. Results are depicted as the mean ± standard error of the mean ($\overline{x}$±SEM).

It is crucial to emphasize that despite the uniform volume content of metallic particles in all composite materials (6.5 vol%), this content translates to different weight percentages: 5 wt% of Mg, 28 wt% of FeMg, and 31.5 wt% of Fe. Consequently, the samples containing Fe-based particles possess nearly three times the moles of the metallic corroding phase in comparison to PLLA/Mg samples (factoring in the molecular weight of Mg at 24.3 g/mol and Fe at 55.8 g/mol, yielding a molar ratio of 2.74 between moles of Fe and moles of Mg within the same volume). However, the alteration in mass of immersed PLLA/Fe samples corresponded similarly to the change observed in PLLA/Mg samples. This could be attributed to the relatively slower degradation rate of Fe when compared to Mg.

Apart from the weight increase attributed to the formation of Fe and Mg degradation products, the substantial presence of P and C, as observed through the EDS technique, suggests the adsorption of these compounds leading to the creation of Fe and Mg phosphates and carbonates. This phenomenon has been similarly documented by Moravej et al. [39] and Zhang et al. [40].

To understand the mechanical response of the degraded composites, various factors warrant consideration. Among these, the interaction between the solution and the matrix and particles, the uniformity of reinforcement distribution, matrix-particle bonding, and the nature and quantity of degradation products all play vital roles. For neat PLLA, hydrolytic degradation leads to the cleavage of polymer chains, resulting in a subsequent reduction in molecular weight and consequently, mechanical strength. The incorporation of metallic particles such as Mg, Fe and FeMg introduces novel modes of degradation. In the case of Mg, the corrosion products manifest as Mg hydroxides and phosphates [12], discernible as white spots on the cylinder surfaces in Fig. 2. The formation of these products triggers an alkaline reaction at the polymer/particle interface, accelerating the hydrolytic degradation of the polymer [41]. Coupled with the degradation of matrix-particle bonding, this mechanism potentially elucidates the lower compressive modulus observed in PLLA/Mg compared to pure PLLA after 28 days of immersion. Regarding PLLA/Fe, the degradation products on the surface adopt a yellowish hue and their dimensions increase with the duration of degradation. These reaction products align with the characteristics of the Fe oxidation process [42–44] further compromising both matrix and interface and contributing to the reduction in mechanical properties after 28 d. Similar mechanisms come into play in the case of PLLA/FeMg, where distinct reaction products contribute to the deterioration of composite integrity. Here, not only does the compressive modulus diminish after 28 days of immersion in PBS, but the compressive yield strength is also inferior to that of the other two composites. This behavior may be attributed to the fact that the

degradation products within PLLA/FeMg are less compact, loosely spread on the cylinder surface, creating expansive polymer-free areas that permit ongoing solution penetration into the matrix. Conversely, in PLLA/Fe, the degradation products cover more extensive portions of the cylinder surfaces, with reduced free areas, seemingly inhibiting the intrusion of the liquid medium.

The mechanism of PLLA degradation involves the diffusion of the liquid medium. The amorphous nature of the PLLA matrix facilitates the diffusion of water within the bulk of the material. The presence of metallic particles like Mg and FeMg enhances water absorption, as evidenced by the water intake data (Fig. 7). While the measurements conducted do not definitively establish that the presence of the metallic particles accelerates PLLA degradation, it was observed that in the case of FeMg particles, the liquid infiltrates the internal volume of the composite specimen, (Fig. 3 (i)). Therefore, it is expected that the interior of the PLLA sample will also undergo hydrolysis upon contact with water, leading to its degradation. This would account the abrupt reduction in both the elastic compressive modulus and yield strength after 28 days of testing in the PLLA/FeMg material. The decline in mechanical strength is comparatively less pronounced in the other materials.

The results of the compressive tests indicated that as-processed composite samples exhibited inferior mechanical properties compared to neat PLLA (Fig. 9). This behavior can most likely be attributed to the uneven distribution and clustering of the reinforcing particles, which lead to the initiation of cracks and premature failures. Jian and Ning [45] demonstrated that incorporating 316 L metal powder as reinforcement for PLLA significantly enhances its compressive modulus and strength by several magnitudes. However, their study also revealed that composites with particle agglomeration exhibited poorer performance in comparison to those with well-dispersed particle.

The microstructural analysis of PLLA/Fe (Fig. 3d), revealed non-uniform distribution of Fe particles within the matrix, with presence of Fe aggregates. Similar microstructural characteristics were observed in PLLA/FeMg samples when compared to PLLA/Fe specimens. Aggregates near the surface were also evident (Fig. 3g). The uneven dispersion of the reinforcement due to particle agglomeration remains a notable concern in the production of biomedical composites [46], as underscored by Wang [47]. The agglomeration observed in the samples could be attributed to their small particle size and the interactions between them. This phenomenon might involve electrostatic and van der Waals forces or the creation of liquid bridges during the composite fabrication process. Interestingly, such agglomeration tendencies were absent in as-processed PLLA/Mg samples (Fig. 3a). A bigger particle size, spherical morphology and a uniform particle size distribution in Mg samples could account for this improved homogeneity when compared to Fe samples. Consequently, in order to enhance the mechanical properties of PLLA composites, a consistent and uniform distribution of the reinforcement is imperative.

Composites reinforced with Fe-containing particles exhibit superior cytocompatibility compared to PLLA/Mg. Remarkably, the cytocompatibility of PLLA/Mg is notably poor, likely due to the release of Mg^{2+} ions reaching cytotoxic levels. This particular composite contains a higher mass of Mg in comparison to PLLA/FeMg. On the other hand, the cytocompatibility of PLLA/FeMg stands out as the most favorable among the composite materials, suggesting that the incorporation of Mg into Fe yields a beneficial effect. During the degradation of the PLLA/Mg composite, a continuous release of Mg and OH^- ions occurs into the surrounding medium. The elevated quantities of these products adversely impact cell viability, resulting in reduced cytocompatibility of the material. In support of this, Li et al. [48] have documented that human osteosarcoma cells (MG-63) did not survive direct contact with a pure Mg scaffold, while other researchers have demonstrated a decline in cell viability in the proximity of pure Mg [49]. However, composites made of PLGA polymer and Mg alloys (such as AZ31, which possesses a slower degradation rate than pure Mg) have exhibited the ability to support the adherence and proliferation of MC3T3 cells. This emphasizes the relevance of the concentration of released Mg^{2+} and OH^- ions in influencing cytocompatibility [50].

The decrease in cytocompatibility observed in PLLA/Fe in comparison to PLLA is consistent with findings from other researchers [51]. These studies demosntrated that when MG-63 cells came into direct contact with pure Fe scaffolds, it led to rapid cytotoxicity. Earlier studies have attributed these harmful outcomes to an excessive presence of Fe, which arises due to the buildup of insoluble degradation products within the cells [36,52].

Even though the mortality rate in PLLA/FeMg resembles that of PLLA/Fe, which is expected due to the similar Fe content in both composites, the advantage of PLLA/FeMg lies in the greater number of cells that manage to adhere to its surface. The inclusion of this modest percentage of Mg within the Fe lattice not only accelerates the degradation of Fe but also enhances its cytocompatibility, making it more akin to the cytocompatibility of the PLLA control. Consistently, a composite material made of β-tricalcium phosphate with Fe and Mg (TCP15Fe15Mg) has been demonstrated to facilitate the attachment, proliferation and differentiation of osteoblast cells [26]. The favorable osteoconductive properties of Mg have been extensively documented in the literature for various Mg-based biomaterials [53–58]. Furthermore, the role of Mg in influencing the expression of vimentin and ICAM-1 proteins in osteoblasts, along with its connection to heightened cell-cell and cell-surface adhesion, has also been reported [59].

Shuai et al. studied various materials to develop electrically conductive channels, a feature necessary in nerve and osteogenic repair. For instance, these researchers have elaborated a scaffold based on PLLA with Sr^{2+}-modified hydroxyapatite with the aim to achieve a material with sustained release of Sr^{2+} over time. This ion stimulated osteogenesis and inhibited osteoclast resorption [60]. Also, to accelerate the degradation of composite materials utilizing PLLA/hydroxyapatite (HAP), the authors demonstrated the efficacy of incorporating polyglycolic acid (PGA). This addition enabled the achievement of an elevated degradation rate while upholding a positive impact on bone defect repair [61]. Although PLLA is not inherently electrically conductive, the use of metallic fillers, such as FeMg particles proposed in the present work, is considered an effective strategy to impart additional electrical conductivity to the polymer [62]. Therefore, the composite material proposed here can be deemed suitable not only for bone regeneration but also for nerve conduction.

5. Conclusions

In the domain of material analysis, microstructural evaluations have been discussed, revealing the critical role of particle distribution in determining mechanical properties. The consistent observation of non-uniform distribution and aggregation of reinforcing particles in composite matrices has been highlighted. It is clear that achieving homogeneity in particle dispersion is necessary to enhancing the mechanical integrity of these composites.

PLLA/FeMg have shown the fastest degradation, as evident from the visual examination of specimens tested in PBS for 14 and 28 days. In this composite, reaction products have emerged throughout the entire specimen volume, resulting in swelling and an increase in sample weight. Additionally, they have exhibited a greater water absorption, indicating the degradation of polymer chains. Conversely, the slower degradation observed in PLLA/Fe can be attributed to a formation of a protective layer on the surface, that impeded the diffusion of degradation media, resulting in a slower degradation process.

The results of the compressive test indicate that the as-processed reinforced specimens exhibit lower mechanical properties compared to those of neat PLLA. This behavior can be attributed to the heterogeneous distribution and agglomeration of the reinforcing particles, these causes initial crack points and premature failures. However, the composites have maintained their initial mechanical properties after 14 days of immersion, in contrast to the behavior observed in PLLA. In the specific case of PLLA/FeMg, these properties have experienced a significant decline after 28 days, which would be suitable for implants with a requirement of a short lifespan.

Direct cytotoxicity assays have demonstrated the ability of pre-osteoblast MC3T3-E1 cells to adhere and proliferate on the surface of PLLA/FeMg. The osteoconductive characteristics of Mg, along with its favorable influence in the adhesion process of osteoblast, position this material as a candidate for integration into orthopedic biomedical devices. Its potential to enhance implant osseointegration and, possibly, nerve conduction, makes it an appealing option for advancing orthopedic applications.

Data availability statement

Data associated with the study has not been deposited into a publicly available repository. Most of the data are included in the manuscript, any other data will be made available on request.

Additional information

No additional information is available for this paper.

CRediT authorship contribution statement

Rafael Guillermo Estrada: Conceptualization, Data curation, Formal analysis, Investigation, Validation, Visualization, Writing – original draft. **Marta Multigner:** Conceptualization, Data curation, Formal analysis, Investigation, Validation, Visualization, Writing – review & editing. **Natalia Fagali:** Data curation, Formal analysis, Investigation, Visualization, Writing – original draft, Writing – review & editing. **Rosa María Lozano:** Funding acquisition, Project administration, Supervision. **Marta Muñoz:** Investigation, Methodology, Resources. **Sandra Carolina Cifuentes:** Formal analysis, Validation, Writing – review & editing. **Belén Torres:** Funding acquisition, Project administration, Supervision. **Marcela Lieblich:** Conceptualization, Data curation, Formal analysis, Funding acquisition, Investigation, Methodology, Project administration, Resources, Supervision, Validation, Visualization, Writing – review & editing.

Declaration of generative AI and AI-assisted technologies in the writing process

During the preparation of this work the authors used Chat GPT in order to improve English grammar. After using this tool/service, the authors reviewed and edited the content as needed and takes full responsibility for the content of the publication.

Declaration of competing interest

The authors declare that they have no known competing financial interests or personal relationships that could have appeared to influence the work reported in this paper.

Acknowledgments

Financial support of Ministry of Science and Innovation of Spain (MICINN) PID2019-104351GB-C21, PCIN-2017-036 (M-ERA-Net2016:4128, EU-FEDER), PID2021-124341OB-C21 and PID2021-123891OB-I00, are greatly acknowledged. R. E. thanks MICINN for the FPI grant PRE2020-092118. The authors thanks CONICET (External Fellowship of NSF, PIP 2021 11220200100315CO), ANPCyT (PICT 2019-0631, PICT Start Up 2020-0034, PICT 2020–02169), UNLP (11/X900), RTI2018-101506-B-C33 from the Ministerio de Ciencia, Innovación y Universidades (MICIU/FEDER), from Spain. The authors thanks J.A. Jiménez and I. Llorente (XRD), M. Maher and A. Tomás (SEM-EDS), M. Acedo (machining) and the students J. Terreros, A. Cardeña and C. Rodríguez-Castañeda (BM).

References

[1] P.B. Maurus, C.C. Kaeding, Bioabsorbable implant material review, Operat. Tech. Sports Med. 12 (2004) 158–160, https://doi.org/10.1053/j.otsm.2004.07.015.

[2] A.D. Banjo, V. Agrawal, M.L. Auad, A.D.N. Celestine, Moisture-induced changes in the mechanical behavior of 3D printed polymers, Composites Part C: Open Access 7 (2022), 100243, https://doi.org/10.1016/J.JCOMC.2022.100243.

[3] R. Suuronen, T. Pohjonen, J. Hietanen, C. Lindqvist, A 5-year in vitro and in vivo study of the biodegradation of polylactide plates, J. Oral Maxillofac. Surg. 56 (1998) 604–614, https://doi.org/10.1016/S0278-2391(98)90461-X.

[4] P. Feng, R. Zhao, W. Tang, F. Yang, H. Tian, S. Peng, et al., Structural and functional adaptive artificial bone: materials, fabrications, and properties, Adv. Funct. Mater. 33 (2023), 2214726, https://doi.org/10.1002/adfm.202214726.

[5] C. Shuai, B. Peng, P. Feng, L. Yu, R. Lai, A. Min, In situ synthesis of hydroxyapatite nanorods on graphene oxide nanosheets and their reinforcement in biopolymer scaffold, J. Adv. Res. 35 (2022) 13–24, https://doi.org/10.1016/J.JARE.2021.03.009.

[6] C. Shuai, G. Liu, Y. Yang, F. Qi, S. Peng, W. Yang, et al., A strawberry-like Ag-decorated barium titanate enhances piezoelectric and antibacterial activities of polymer scaffold, Nano Energy 74 (2020), 104825, https://doi.org/10.1016/J.NANOEN.2020.104825.

[7] K. Rezwan, Q.Z. Chen, J.J. Blaker, A.R. Boccaccini, Biodegradable and bioactive porous polymer/inorganic composite scaffolds for bone tissue engineering, Biomaterials 27 (2006) 3413–3431, https://doi.org/10.1016/J.BIOMATERIALS.2006.01.039.

[8] M. Navarro, M.P. Ginebra, J.A. Planell, C.C. Barrias, M.A. Barbosa, In vitro degradation behavior of a novel bioresorbable composite material based on PLA and a soluble CaP glass, Acta Biomater. 1 (2005) 411–419, https://doi.org/10.1016/J.ACTBIO.2005.03.004.

[9] Y.F. Zheng, X.N. Gu, F. Witte, Biodegradable metals, Mater. Sci. Eng. R Rep. 77 (2014) 1–34, https://doi.org/10.1016/J.MSER.2014.01.001.

[10] R. Gorejová, L. Haverová, R. Oriňaková, A. Oriňak, M. Oriňak, Recent advancements in Fe-based biodegradable materials for bone repair, J. Mater. Sci. 54 (2019) 1913–1947, https://doi.org/10.1007/s10853-018-3011-z.

[11] E. Mostaed, M. Sikora-Jasinska, J.W. Drelich, M. Vedani, Zinc-based alloys for degradable vascular stent applications, Acta Biomater. 71 (2018) 1–23, https://doi.org/10.1016/J.ACTBIO.2018.03.005.

[12] S.C. Cifuentes, R. Gavilán, M. Lieblich, R. Benavente, J.L. González-Carrasco, In vitro degradation of biodegradable polylactic acid/magnesium composites: relevance of Mg particle shape, Acta Biomater. 32 (2016) 348–357, https://doi.org/10.1016/J.ACTBIO.2015.12.037.

[13] C. Zhao, H. Wu, J. Ni, S. Zhang, X. Zhang, Development of PLA/Mg composite for orthopedic implant: tunable degradation and enhanced mineralization, Compos. Sci. Technol. 147 (2017) 8–15, https://doi.org/10.1016/J.COMPSCITECH.2017.04.037.

[14] X. Li, C. Chu, Y. Wei, C. Qi, J. Bai, C. Guo, et al., In vitro degradation kinetics of pure PLA and Mg/PLA composite: effects of immersion temperature and compression stress, Acta Biomater. 48 (2017) 468–478, https://doi.org/10.1016/J.ACTBIO.2016.11.001.

[15] S.C. Cifuentes, M. Lieblich, L. Saldaña, J.L. González-Carrasco, R. Benavente, In vitro degradation of biodegradable polylactic acid/Mg composites: influence of nature and crystalline degree of the polymeric matrix, Materialia (Oxf) 6 (2019), 100270, https://doi.org/10.1016/J.MTLA.2019.100270.

[16] C. Shuai, Y. Li, P. Feng, W. Guo, W. Yang, S. Peng, Positive feedback effects of Mg on the hydrolysis of poly-l-lactic acid (PLLA): promoted degradation of PLLA scaffolds, Polym. Test. 68 (2018) 27–33, https://doi.org/10.1016/J.POLYMERTESTING.2018.03.042.

[17] N. Argarate, B. Olalde, G. Atorrasagasti, J. Valero, S. Carolina Cifuentes, R. Benavente, et al., Biodegradable Bi-layered coating on polymeric orthopaedic implants for controlled release of drugs, Mater. Lett. 132 (2014) 193–195, https://doi.org/10.1016/J.MATLET.2014.06.070.

[18] S.C. Cifuentes, E. Frutos, J.L. González-Carrasco, M. Muñoz, M. Multigner, J. Chao, et al., Novel PLLA/magnesium composite for orthopedic applications: a proof of concept, Mater. Lett. 74 (2012) 239–242, https://doi.org/10.1016/J.MATLET.2012.01.134.

[19] A. Ferrández-Montero, M. Lieblich, J.L. González-Carrasco, R. Benavente, V. Lorenzo, R. Detsch, et al., Development of biocompatible and fully bioabsorbable PLA/Mg films for tissue regeneration applications, Acta Biomater. 98 (2019) 114–124, https://doi.org/10.1016/J.ACTBIO.2019.05.026.

[20] A. Brown, S. Zaky, H. Ray, C. Sfeir, Porous magnesium/PLGA composite scaffolds for enhanced bone regeneration following tooth extraction, Acta Biomater. 11 (2015) 543–553, https://doi.org/10.1016/J.ACTBIO.2014.09.008.

[21] L. Xu, A. Yamamoto, In vitro degradation of biodegradable polymer-coated magnesium under cell culture condition, Appl. Surf. Sci. 258 (2012) 6353–6358, https://doi.org/10.1016/J.APSUSC.2012.03.036.

[22] S.C. Cifuentes, F. Bensiamar, A.M. Gallardo-Moreno, T.A. Osswald, J.L. González-Carrasco, R. Benavente, et al., Incorporation of Mg particles into PDLLA regulates mesenchymal stem cell and macrophage responses, J. Biomed. Mater. Res. 104 (2016) 866–878, https://doi.org/10.1002/jbm.a.35625.

[23] Y. Guangyin, N. Jialin, Medical Degradable Fe-Mg Binary Alloy Material and Preparation Method Thereof, CN103028149B, 2012.

[24] M. Multigner, M. Lieblich, J.L. González-Carrasco, A. Rodríguez-Castañeda, P. de la Presa, J. Rams, Characterization of planetary ball-milled Fe-Mg powder, in: Proceedings of the 11th International Symposium on Biodegradable Metals for Biomedical Applications, Biometal, Alicante, 2019.

[25] R. Oriňáková, A. Oriňák, L.M. Bučková, M. Giretová, Medvecký Ľ, E. Labbanczová, et al., Iron Based Degradable Foam Structures for Potential Orthopedic Applications, vol. 8, 2013.

[26] S.K. Swain, I. Gotman, R. Unger, C.J. Kirkpatrick, E.Y. Gutmanas, Microstructure, mechanical characteristics and cell compatibility of β-tricalcium phosphate reinforced with biodegradable Fe–Mg metal phase, J. Mech. Behav. Biomed. Mater. 53 (2016) 434–444, https://doi.org/10.1016/J.JMBBM.2015.09.002.

[27] G. Xie, H. Takada, H. Kanetaka, Development of high performance MgFe alloy as potential biodegradable materials, Mater. Sci. Eng. 671 (2016) 48–53, https://doi.org/10.1016/j.msea.2016.06.051.

[28] C. Shuai, C. He, G. Qian, A. Min, Y. Deng, W. Yang, et al., Mechanically driving supersaturated Fe–Mg solid solution for bone implant: preparation, solubility and degradation, Compos. B Eng. (2021) 207, https://doi.org/10.1016/j.compositesb.2020.108564.

[29] R.G. Estrada, M. Multigner, M. Lieblich, S. Fajardo, J. Rams, Effect of magnesium addition and high energy processing on the degradation behavior of iron powder in modified Hanks' solution for bioabsorbable implant applications, Metals 12 (2022), https://doi.org/10.3390/met12010078.

[30] M. Schinhammer, A.C. Hänzi, J.F. Löffler, P.J. Uggowitzer, Design strategy for biodegradable Fe-based alloys for medical applications, Acta Biomater. 6 (2010) 1705–1713, https://doi.org/10.1016/j.actbio.2009.07.039.

[31] K. Kawaguchi, R. Yamamoto, N. Hosoito, T. Shinjo, T. Takada, Magnetic properties of Fe–Mg artificial superstructure films, J. Physical Soc. Japan 55 (1986) 2375–2383.

[32] A. Fnidiki, J.P. Eymery, M.F. Denanot, Structure and stability of Fe−Mg amorphous alloys prepared by coevaporation, Hyperfine Interact. 45 (1989) 295–300, https://doi.org/10.1007/BF02405891.

[33] A. Hightower, B. Fultz, R.C. Bowman, Mechanical alloying of Fe and Mg, J. Alloys Compd. 252 (1997) 238–244, https://doi.org/10.1016/S0925-8388(96)02732-6.

[34] S.C. Cifuentes, M. Lieblich, F.A. López, R. Benavente, J.L. González-Carrasco, Effect of Mg content on the thermal stability and mechanical behaviour of PLLA/Mg composites processed by hot extrusion, Mater. Sci. Eng. C 72 (2017) 18–25, https://doi.org/10.1016/J.MSEC.2016.11.037.

[35] L.T. Lim, R. Auras, M. Rubino, Processing technologies for poly(lactic acid), Prog. Polym. Sci. 33 (2008) 820–852, https://doi.org/10.1016/J.PROGPOLYMSCI.2008.05.004.

[36] N.S. Fagali, M.A. Madrid, B.T. Pérez Maceda, M.E. López Fernández, R.M. Lozano Puerto, M. Fernández Lorenzo de Mele, Effect of degradation products of iron-bioresorbable implants on the physiological behavior of macrophages in vitro, Metallomics 12 (2020) 1841–1850, https://doi.org/10.1039/d0mt00151a.

[37] F Von Burkersroda, L. Schedl, A. Göpferich, Why degradable polymers undergo surface erosion or bulk erosion, Biomaterials 23 (2002) 4221–4231, https://doi.org/10.1016/S0142-9612(02)00170-9.

[38] K. Chen, K.S. Schweizer, Theory of yielding, strain softening, and steady plastic flow in polymer glasses under constant strain rate deformation, Macromolecules 44 (2011) 3988–4000, https://doi.org/10.1021/ma200436w.

[39] M. Moravej, A. Purnama, M. Fiset, J. Couet, D. Mantovani, Electroformed pure iron as a new biomaterial for degradable stents: in vitro degradation and preliminary cell viability studies, Acta Biomater. 6 (2010) 1843–1851, https://doi.org/10.1016/J.ACTBIO.2010.01.008.

[40] E. Zhang, H. Chen, F. Shen, Biocorrosion properties and blood and cell compatibility of pure iron as a biodegradable biomaterial, J. Mater. Sci. Mater. Med. 21 (2010) 2151–2163, https://doi.org/10.1007/s10856-010-4070-0.
[41] H. Tsuji, Y. Ikada, Properties and morphology of poly(L-lactide). II. Hydrolysis in alkaline solution, J. Polym. Sci. Polym. Chem. 36 (1998) 59–66, https://doi.org/10.1002/(SICI)1099-0518(19980115)36:1<59::AID-POLA9>3.0.CO;2-X.
[42] J. Kassim, T. Baird, J.R. Fryer, Electron microscope studies of iron corrosion products in water at room temperature, Corrosion Sci. 22 (1982) 147–158, https://doi.org/10.1016/0010-938X(82)90075-0.
[43] M. Usman, J.M. Byrne, A. Chaudhary, S. Orsetti, K. Hanna, C. Ruby, et al., Magnetite and green rust: synthesis, properties, and environmental applications of mixed-valent iron minerals, Chem. Rev. 118 (2018) 3251–3304, https://doi.org/10.1021/acs.chemrev.7b00224.
[44] F. Bocher, A. Géhin, C. Ruby, J. Ghanbaja, M. Abdelmoula, J.M.R. Génin, Coprecipitation of Fe(II–III) hydroxycarbonate green rust stabilised by phosphate adsorption, Solid State Sci. 6 (2004) 117–124, https://doi.org/10.1016/J.SOLIDSTATESCIENCES.2003.10.004.
[45] D. Jiang, F. Ning, Fused filament fabrication of biodegradable PLA/316L composite scaffolds: effects of metal particle content, Procedia Manuf. 48 (2020) 755–762, https://doi.org/10.1016/J.PROMFG.2020.05.110.
[46] H. Zhou, J.G. Lawrence, S.B. Bhaduri, Fabrication aspects of PLA-CaP/PLGA-CaP composites for orthopedic applications: a review, Acta Biomater. 8 (2012) 1999, https://doi.org/10.1016/J.ACTBIO.2012.01.031. –2016.
[47] M. Wang, Developing bioactive composite materials for tissue replacement, Biomaterials 24 (2003) 2133–2151, https://doi.org/10.1016/S0142-9612(03)00037-1.
[48] Y. Li, J. Zhou, P. Pavanram, M.A. Leeflang, L.I. Fockaert, B. Pouran, et al., Additively manufactured biodegradable porous magnesium, Acta Biomater. 67 (2018) 378–392, https://doi.org/10.1016/J.ACTBIO.2017.12.008.
[49] C.A. Grillo, F. Alvarez, M.A. Fernández Lorenzo De Mele, Degradation of bioabsorbable Mg-based alloys: assessment of the effects of insoluble corrosion products and joint effects of alloying components on mammalian cells, Mater. Sci. Eng. C 58 (2016) 372–380, https://doi.org/10.1016/J.MSEC.2015.08.043.
[50] Y.H. Wu, N. Li, Y. Cheng, Y.F. Zheng, Y. Han, In vitro study on biodegradable AZ31 magnesium alloy fibers reinforced PLGA composite, J. Mater. Sci. Technol. 29 (2013) 545–550, https://doi.org/10.1016/J.JMST.2013.03.004.
[51] Y. Li, H. Jahr, K. Lietaert, P. Pavanram, A. Yilmaz, L.I. Fockaert, et al., Additively manufactured biodegradable porous iron, Acta Biomater. 77 (2018) 380–393, https://doi.org/10.1016/J.ACTBIO.2018.07.011.
[52] N.S. Fagali, C.A. Grillo, S. Puntarulo, M.A. Fernández Lorenzo de Mele, Is there any difference in the biological impact of soluble and insoluble degradation products of iron-containing biomaterials? Colloids Surf. B Biointerfaces 160 (2017) 238–246, https://doi.org/10.1016/J.COLSURFB.2017.09.032.
[53] C. Castellani, R.A. Lindtner, P. Hausbrandt, E. Tschegg, S.E. Stanzl-Tschegg, G. Zanoni, et al., Bone–implant interface strength and osseointegration: biodegradable magnesium alloy versus standard titanium control, Acta Biomater. 7 (2011) 432–440, https://doi.org/10.1016/J.ACTBIO.2010.08.020.
[54] C. Janning, E. Willbold, C. Vogt, J. Nellesen, A. Meyer-Lindenberg, H. Windhagen, et al., Magnesium hydroxide temporarily enhancing osteoblast activity and decreasing the osteoclast number in peri-implant bone remodelling, Acta Biomater. 6 (2010) 1861–1868, https://doi.org/10.1016/J.ACTBIO.2009.12.037.
[55] M. Alvarez-Lopez, M.D. Pereda, J.A. Del Valle, M. Fernandez-Lorenzo, M.C. Garcia-Alonso, O.A. Ruano, et al., Corrosion behaviour of AZ31 magnesium alloy with different grain sizes in simulated biological fluids, Acta Biomater. 6 (2010) 1763–1771, https://doi.org/10.1016/J.ACTBIO.2009.04.041.
[56] A. Oriňák, R. Oriňáková, Z.O. Králová, A.M. Turoňová, M. Kupková, M. Hrubovčáková, et al., Sintered metallic foams for biodegradable bone replacement materials, J. Porous Mater. 21 (2014) 131–140, https://doi.org/10.1007/s10934-013-9757-4.
[57] H. Zhou, B. Liang, H. Jiang, Z. Deng, K. Yu, Magnesium-based biomaterials as emerging agents for bone repair and regeneration: from mechanism to application, J. Magnesium Alloys 9 (2021) 779–804, https://doi.org/10.1016/J.JMA.2021.03.004.
[58] S. Galli, M. Stocchero, M. Andersson, J. Karlsson, W. He, T. Lilin, et al., The effect of magnesium on early osseointegration in osteoporotic bone: a histological and gene expression investigation, Osteoporos. Int. 28 (2017) 2195–2205, https://doi.org/10.1007/s00198-017-4004-5.
[59] F. Alvarez, R.M. Lozano Puerto, B. Pérez-Maceda, C.A. Grillo, M. Fernández Lorenzo de Mele, Time-lapse evaluation of interactions between biodegradable Mg particles and cells, Microsc. Microanal. 22 (2016) 1–12, https://doi.org/10.1017/S1431927615015597.
[60] F. Qi, Z. Wang, Y. Shuai, S. Peng, C. Shuai, Sr2+ sustained release system augments bioactivity of polymer scaffold, ACS Appl. Polym. Mater. 4 (2022) 2691–2702, https://doi.org/10.1021/acsapm.2c00024.
[61] C. Shuai, W. Yang, P. Feng, S. Peng, H. Pan, Accelerated degradation of HAP/PLLA bone scaffold by PGA blending facilitates bioactivity and osteoconductivity, Bioact. Mater. 6 (2021) 490–502, https://doi.org/10.1016/J.BIOACTMAT.2020.09.001.
[62] F. Qi, R. Liao, Y. Shuai, H. Pan, G. Qian, S. Peng, et al., A conductive network enhances nerve cell response, Addit. Manuf. 52 (2022), 102694, https://doi.org/10.1016/J.ADDMA.2022.102694.